



CHORUS

This is the accepted manuscript made available via CHORUS. The article has been published as:

Antiferromagnetic order in single crystals of the $S=2$ quasi-one-dimensional chain $\text{MnCl}_3(\text{bpy})$

Shin-ichi Shinozaki, Akira Okutani, Daichi Yoshizawa, Takanori Kida, Tetsuya Takeuchi, Shoji Yamamoto, Olivia N. Risset, Daniel R. Talham, Mark W. Meisel, and Masayuki Hagiwara

Phys. Rev. B **93**, 014407 — Published 8 January 2016

DOI: [10.1103/PhysRevB.93.014407](https://doi.org/10.1103/PhysRevB.93.014407)

Antiferromagnetic Order in Single Crystals of the $S = 2$ Quasi-linear Chain $\text{MnCl}_3(\text{bpy})$

Shin-ichi Shinozaki¹, Akira Okutani¹, Daichi Yoshizawa¹, Takanori Kida¹, Tetsuya Takeuchi², Shoji Yamamoto³, Olivia N. Risset⁴, Daniel R. Talham⁴, Mark W. Meisel⁵, and Masayuki Hagiwara¹

¹*Center for Advanced High Magnetic Field Science, Graduate School of Science, Osaka University, Toyonaka, Osaka 560-0043, Japan*

²*Low Temperature Center, Osaka University, Toyonaka, Osaka 560-0043, Japan*

³*Department of Physics, Hokkaido University, Sapporo, Hokkaido 060-0810, Japan*

⁴*Department of Chemistry, University of Florida, Gainesville, FL 32611-7200, USA*

⁵*Department of Physics and the National High Magnetic Field Laboratory, University of Florida, Gainesville, FL 32611-8440, USA*

(Dated: December 2, 2015)

A suite of experimental tools, including high-field magnetization and electron spin resonance (ESR) studies in magnetic fields of up to 50 T and heat capacity studies up to 9 T, have revealed antiferromagnetic order in single crystals of the Heisenberg $S = 2$ chain compound $\text{MnCl}_3(\text{bpy})$, where bpy is 2,2'-bipyridine. The Néel temperature, which depends on the strength of the applied magnetic field and its orientation with respect to the crystalline axes that was revealed by heat capacity measurements, is near 11.5 K in zero field. The spin-flop transition is identified in the magnetization curve acquired at 1.7 K and at $\mu_0 H_{\text{SF}}^c = 24$ T along the c -axis. The transition field H_{SF} is lower than that expected from the previous antiferromagnetic resonance (AFMR) studies on a powder sample. The identification of the long-range antiferromagnetic order resolves an earlier report by Granroth *et al.* [Phys. Rev. Lett. **77**, 1616 (1996)] that identified $\text{MnCl}_3(\text{bpy})$ as an $S = 2$ Haldane system down to 40 mK. The ESR studies identify a wide-range of antiferromagnetic resonance modes that provide additional microscopic information about the g -values ($g_{a^*} = 2.09$, $g_b = 1.92$, and $g_c = 2.07$), the zero-field splitting constants, $D = -1.5$ K and $E = -0.17$ K when the nearest-neighbor spin interaction $J/k_B = 31.2$ K, which is evaluated from fitting the susceptibility, and the anisotropy of this compound (easy-axis is the c -axis, the second easy-axis is the b -axis, and the hard axis is the a^* -axis), when using a standard (two-sublattices) AFMR analysis that does not quantitatively reproduce the observed H_{SF}^c values. The observed resonance mode indicates the frequency minimum at H_{SF}^c .

PACS numbers: 75.50.Ee, 75.30.Cr, 76.50.+g, 75.40.Cx

I. INTRODUCTION

The quantum nature of linear-chain Heisenberg antiferromagnets (LCHAs) with spin quantum number $S = 1/2$ dates back to the early years of quantum mechanics, when Bethe provided a first solution.¹ Although a number of researchers clarified issues related to Bethe's ansatz,^{2,3} a revolution occurred when Haldane identified the differences between half-integer and integer spin chains.⁴ Specifically, while the half-integer spin chains were indeed described by the preceding work,^{2,3,5-8} the integer spin chain possessed an energy gap,⁴ where $\Delta_{S=1} \approx 0.41J$ for $S = 1$ LCHAs without anisotropic terms.⁹⁻¹¹ Here, $J(> 0)$ is the nearest-neighbor intrachain magnetic superexchange parameter, and the spin Hamiltonian, which defines the notation for J , λ , D , E , and g , is

$$\mathcal{H} = J \sum_i \{ [S_i^x S_{i+1}^x + S_i^y S_{i+1}^y + \lambda S_i^z S_{i+1}^z] + D(S_1^z)^2 + E[(S_i^x)^2 - (S_i^y)^2] \} - \mathbf{H} \cdot \tilde{g} \cdot \mathbf{S} \quad (1)$$

where λ is a parameter distorting the exchange interaction, D and E are the single-ion and rhombic anisotropies that are commonly referred to as zero-field splitting pa-

rameters arising from the crystal-field anisotropy, \tilde{g} is the g -factor tensor, and \mathbf{H} is the applied magnetic field. Subsequently, theoretical and numerical studies were extended to $S = 2$ chains and provided the Haldane gap $\Delta_{S=2} \approx 0.09J$,^{10,11} the $\lambda - D$ phase diagram,¹²⁻¹⁴ the topological differences between odd and even integer spin chains,^{15,16} and a semiclassical approximation to calculate the ESR properties.¹⁷

Experimentally, a wide-range of studies have investigated $S = 1$ systems,¹⁸⁻²⁵ but only some $S = 2$ materials have been studied in detail,²⁶⁻²⁹ since most systems exhibited a long-range antiferromagnetic order at temperatures that were too high to allow the Haldane gap to be fully developed. One exception was reported by Granroth *et al.*,³⁰ who identified $\text{MnCl}_3(\text{bpy})$ as an $S = 2$ Haldane system down to 40 mK. Motivated to explore the ESR properties of this system, a series of high magnetic field studies were performed on microcrystalline samples at temperatures below 2 K, and the results suggested the presence of long-range antiferromagnetic order.^{31,32} To clarify these results, a number of single-crystals were synthesized and studied. The main features of the data to be presented herein include the identification of a Néel temperature near 11.5 K as resolved by magnetization³³ and heat capacity measurements, and the mapping of the

antiferromagnetic resonance modes over a wide range of frequency, 70 GHz to 1393 GHz, and magnetic fields of up to 53 T. Although the modes of the resonances are well-described by the standard two-sublattice antiferromagnetic resonance (AFMR) model, the c -axis data near and above the spin-flop field H_{SF}^c are not consistent with the predictions.

II. EXPERIMENTAL AND NUMERICAL CALCULATION DETAILS

The synthesis protocol followed procedures described in the literature,³⁴ and these steps were also employed to generate the samples used in earlier work.^{30,35,36} The only potential difference employed in the synthesis of the single crystals reported herein involves the recrystallization procedure. More specifically, after redissolving the powder in acetonitrile at 70 °C, the solution is filtered and left to cool *slowly*. Since the product is rather insoluble in acetonitrile, if cooled too fast, only small crystals are obtained. A standard approach is to recrystallize enough compound to be distributed to ten, 25-ml vials, from which only one typically provides a single crystal. About 20 different crystals, with masses ranging from nominally 1 mg to 2.5 mg, were used for this work.

The magnetic susceptibilities ($\chi = M/B$) and magnetization (M) in fields up to 7 T were measured with a commercial SQUID magnetometer (Quantum Design, MPMS-XL7), and the results were corrected for background contributions. A typical measurement consisted of a single crystal with mass *c.a.* 2~4 mg being glued to a quartz plate to make the measurements with $H||a^*$, c . For $H||b$, the sample was held between two pieces of cotton wool. For the temperature dependent studies, the samples were field-cooled and data were taken while cooling.

Using a standard induction method with a pick-up coil arrangement, the high-field magnetization was studied in pulsed magnetic fields of up to 50 T, and the signal response was calibrated by comparison to the data obtained with the SQUID magnetometer up to 7 T. High-field, multi-frequency (HFMF) ESR measurements in pulsed magnetic fields up to 50 T, with a duration of about 7 ms, utilized a far-infrared laser or some Gunn oscillators with frequency-doublers to generate submillimeter and millimeter waves and a magnetically-tuned InSb hot-electron bolometer as the detector. All of these instruments and resources are located in the AMHF facilities at Osaka University.

The heat capacity was measured by the quasi-adiabatic heat-pulse method in magnetic fields of up to 9 T. A strain gauge heater and a CernoxTM thermometer (Lakeshore Cryogenics) were attached to the back of the sample platform. The CernoxTM sensor was calibrated in magnetic fields against calibrated thermometers maintained by Lakeshore Cryogenics, Inc. Apiezon N grease was used to fix small single crystals to the platform and

five crystals with a total mass of ~ 7.5 mg were utilized for the measurement. The heat capacity of the empty platform was measured in magnetic fields and subtracted from the total measured heat capacity to obtain the heat capacity of the sample.

The magnetic susceptibilities were calculated by a quantum Monte Carlo method for the $S = 2$ LCHA by using the spin Hamiltonian given by Eq. (1) with $\lambda = 1$ and $D = E = 0$. Results for both open (97 spins) and unfrustrated periodic (96 spins) chains were obtained and their thermodynamic properties are well convergent. The details of the calculations are described in Ref. 37.

III. RESULTS AND DISCUSSION

A. Low-field magnetic susceptibility

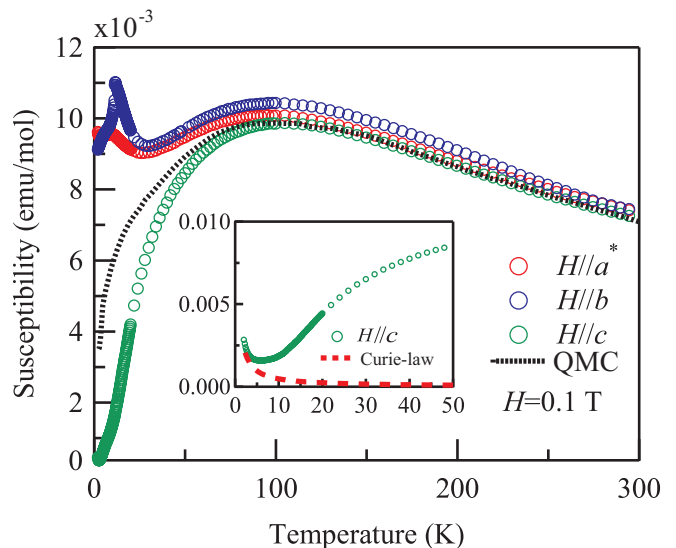


FIG. 1. (Color online) The temperature dependences of the low-field (0.1 T) dc magnetic susceptibilities χ are shown when the field is applied along the a^* , b , and c crystalline axes. The evidence for the long-range order is prominently detected when $H \parallel b$, while the antiferromagnetic nature when $H \parallel c$ is not clearly evidenced. The dotted black line shows the result of a quantum Monte Carlo (QMC) calculation for the $S = 2$ LCHA consisting of 96 spins with periodic boundary conditions using $g = 2.07$ and the $J/k_B = 31.2$ K. The inset shows a small Curie-like low-temperature contribution (Curie-law) that has been subtracted from all of the data in the main panel.

The temperature dependences of low-field (0.1 T) dc magnetic susceptibility χ obtained from a 2.4 mg single-crystal after subtracting the contribution of magnetic impurities are shown in Fig. 1, where an anomalous feature is clearly visible at 11.7 K when $H||b$. As discussed in Ref. 33, this peak can be caused by the canted magnetic moments in the long-range ordered state that exhibits at 11.7 K. The raw results possess a Curie-like tail at the

lowest temperatures as shown in the inset of Fig. 1. The contribution of the magnetic impurities is evaluated by the fitting of the low temperature susceptibility with a Curie formula as indicated by the broken line (calculation) in the inset of Fig. 1. Assuming this contribution arises from trace amounts of Mn^{2+} ions, with $S = 5/2$ and $g = 2$, left during the synthesis, then this contribution might be assigned to $\approx 0.1\%$ of the total spins per mole, which is consistent with the previously reported results.^{30,31,35}

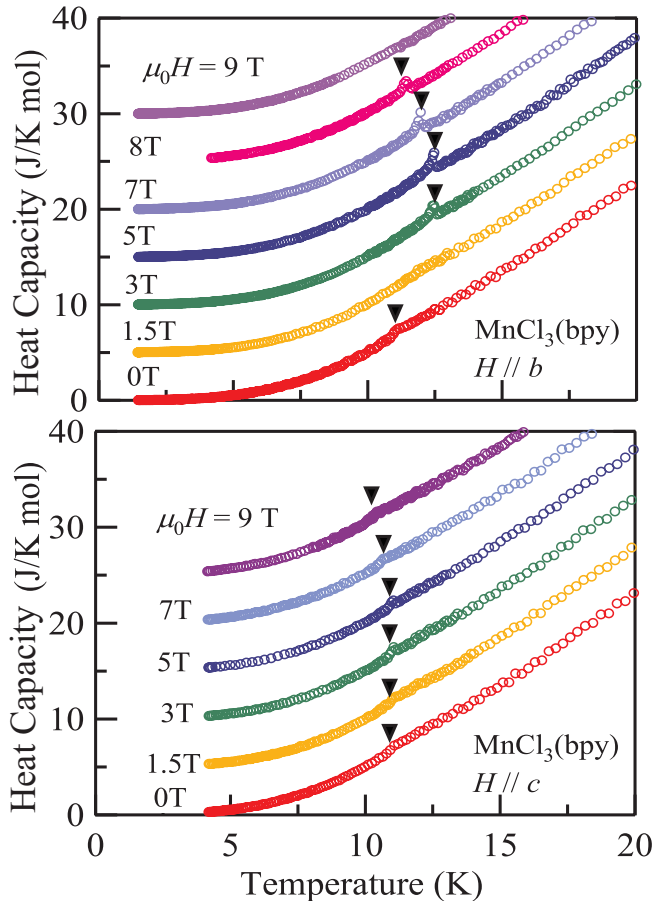


FIG. 2. (Color online) Temperature dependence of heat capacity for the designated magnetic fields up to 9 T for $H||b$ (upper) and $H||c$ (lower). The data sets have been uniformly shifted for clarity.

The magnetic susceptibilities show broad maxima around 100 K for all crystalline directions (a^* , b , and c), which is typical of low dimensional antiferromagnets. Below 100 K, the magnetic susceptibilities are largely different from each other. These results are somewhat similar to the ones reported by Granroth *et al.*,³⁰ who studied a bundle of 90 tiny single crystals whose c -axes were oriented but whose a - and b -axes were randomly mixed. The dotted line in Fig. 1 is the calculated magnetic susceptibility using the parameters $J/k_B = 31.2$ K and $g = 2.07$. The magnetic behavior above 100 K for $H||c$ is well reproduced, but that below 100 K is largely different from

the experimental result, even if one compares the arithmetic means of all the magnetic susceptibilities with the same g -value as in the c -axis.

B. Heat Capacity

The heat capacity data emphasize the transition observed at 11.5 K when $H||b$ is long-ranged in nature and not just an artifact. The two panels of Fig. 2 indicate the temperature dependences of heat capacity for the designated orientations of the magnetic fields, and a tiny peak marked by the inverted triangles around 11.5 K shifts a bit with increasing magnetic field, especially for $H||b$. The peak corresponds to the antiferromagnetic long-range order and is quite small because a significant amount of entropy has already reduced by the well-developed short range order below 100 K. A strikingly similar, small peak has been recently been observed in $\text{MnF}(\text{salen})$, another $S = 2$ linear-chain system.³⁸

C. Magnetization

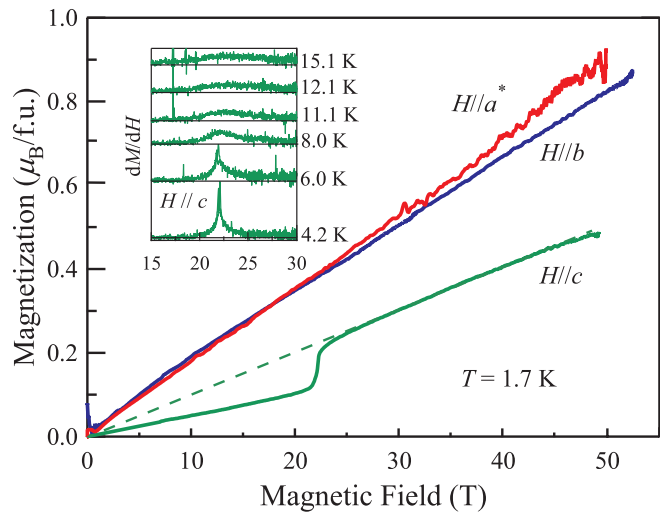


FIG. 3. (Color online) The isothermal ($T = 1.7$ K) magnetization results acquired when the field was oriented along the three crystal axes are shown for fields up to 50 T. The inset shows the temperature dependences of the derivatives of the $H||c$ data sets.

Figure 3 shows magnetization curves at 1.7 K along the a^* , b , and c directions. The magnetization curve for $H||c$ indicates a spin-flop transition at 22 T. Below this transition field, the magnetization possesses a gradual but considerable slope at low enough temperature below T_N , which is not typical for the spin-flop transition in a two-sublattice antiferromagnet. The extrapolated broken line drawn from the high field magnetization goes toward the origin of M - H plot, indicating the spin-flop transition. The large noise of the magnetization for $H||a^*$ at fields

above 25 T was caused by an issue with the pulse magnet. In the inset of the figure, the temperature dependence of the derivative of magnetization with respect to field is shown near the spin-flop transition and indicates the presence of a broad peak above $T_N \approx 11$ K.

D. AFMR

Figure 4 presents the ESR spectra at the lowest temperatures in the measurements for $H||a^*$ (upper left), $H||b$ (lower left), and $H||c$ (right). Downward arrows indicate the resonance fields at designated frequencies. We utilized a transmission-type ESR cryostat, and the signals contain the component of dispersion that deforms the absorption line shape. Therefore, the resonance fields have some uncertainties, which are within the symbol sizes.

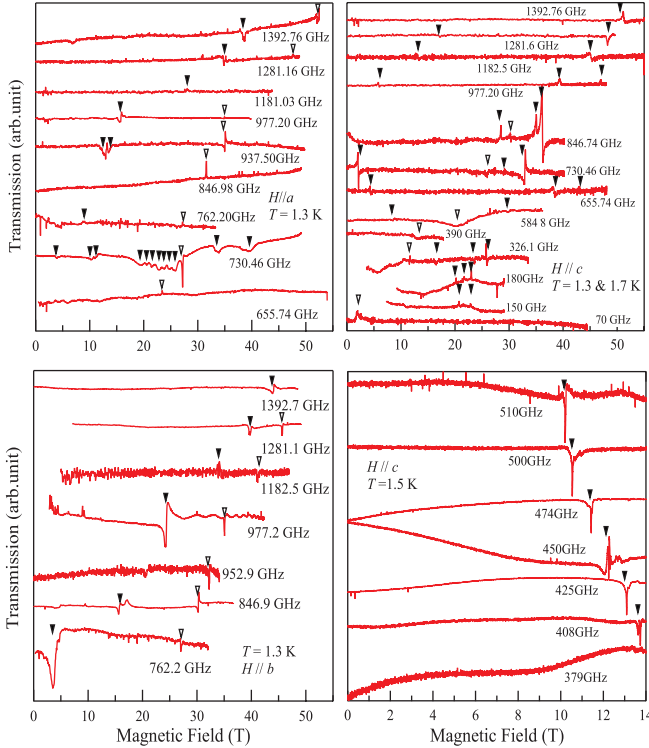


FIG. 4. (Color online) Low temperature ESR spectra for $H||a^*$ at 1.3 K (upper left), $H||b$ at 1.3 K (lower left), and $H||c$ at 1.3 K and 1.7 K (upper right) and at 1.5 K (lower right). Open and closed symbols mark the resonance fields of DPPH (ESR marker with $g=2.0036$) and sample, respectively.

The resonance fields indicated by the downward arrows in Fig. 4 are plotted in the frequency-magnetic field plane as shown in Fig. 5. The broken line in the figure indicates a paramagnetic resonance line with $g = 2$, and some resonance branches other than the paramagnetic resonance line were observed. In the present study, the anisotropy in $\text{MnCl}_3(\text{bpy})$ can be extracted from the resonance modes for each direction. Specifically, these

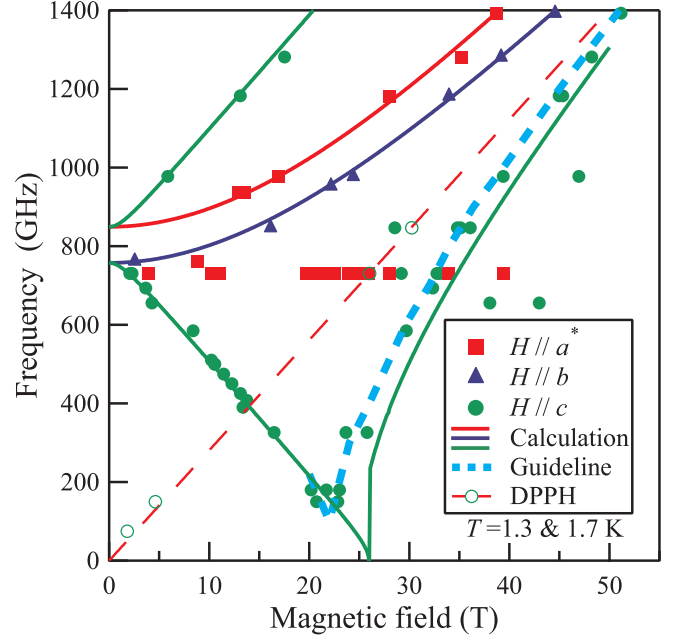


FIG. 5. (Color online) Frequency versus magnetic field plot of the resonance fields indicated in Fig. 4. The broken line is a paramagnetic resonance line with $g = 2$, and the solid lines are antiferromagnetic resonance (AFMR) modes with orthorhombic anisotropy calculated for two-sublattices, see text for the detailed discussion.

modes have two zero-field energy gaps near 800 GHz as also observed with a powder sample,³² and the difference between these gaps is quite small, indicating nearly uniaxial anisotropy. These resonance modes indicate the c , b , a^* -axes are the easy, the second-easy, and the hard axes, respectively. In Fig. 5, the green solid line close to the solid circles is the calculated AFMR mode for the easy axis, and the blue solid line close to the solid triangles and the red solid line close to the solid squares are the AFMR results for the second-easy and the hard axes. The assumptions for our analysis suggested from the AFMR data sets are a negative D value in Eq. (1) and magnetic fields well below the saturation field. The AFMR modes at $T = 0$, except for field-independent resonance modes, are written as:³²

- (1) For $H||z$ (easy axis, c) and $H < H_{SF}$ (H_{SF} is a spin flop field),

$$\left(\frac{\omega_z}{\gamma}\right)^2 = \frac{1}{2}[(2H_z^2 + C_1 + C_2 \pm \sqrt{8H_z^2(C_1 + C_2) + (C_2 - C_1)^2}], \quad (2)$$

- and for $H || z$ (easy axis, c) and $H > H_{SF}$,

$$\left(\frac{\omega_z}{\gamma}\right)^2 = H_z^2 - C_1 \cos^2 \theta. \quad (3)$$

- (2) For $H||x$ (hard axis, a^*),

$$\left(\frac{\omega_x}{\gamma}\right)^2 = H_x^2 + C_2. \quad (4)$$

(3) For $H\parallel y$ (second-easy axis, b),

$$\left(\frac{\omega_y}{\gamma}\right)^2 = H_y^2 + C_1. \quad (5)$$

Here, ω_i ($i = z$ or x or y) is the angular frequency for the i direction, γ is the gyromagnetic ratio for a free electron, $H_i = \frac{g_i}{2}H$ ($i = x$ or y or z , H is the external field),

$$C_1 = 2AK_1, \quad (6)$$

$$C_2 = 2AK_2, \quad (7)$$

and

$$A = \frac{zJ}{(g\mu_B)^2} \left(\frac{2}{N}\right), \quad (8)$$

$$K_1 = (-D - E)NS(S - 1/2);, \quad (9)$$

$$K_2 = (-D + E)NS(S - 1/2). \quad (10)$$

The $\cos^2 \theta$ in Eq. (3) is defined as

$$\cos^2 \theta = 1 - \left(\frac{H_{SF} + H_{A1}}{2H_E}\right)^2, \quad (11)$$

$$H_{SF} = \sqrt{C_1}, \quad (12)$$

$$H_{A1} = K_1/M_0, \quad (13)$$

$$H_E = AM_0, \quad (14)$$

$$M_0 = Ng\mu_B S/2, \quad (15)$$

where A is the molecular field constant of the two-sublattice, N is the number of magnetic ions, z is the number of neighboring sites, and K_1 and K_2 are the anisotropy constants for the second-easy axis and the hard axis, respectively.^{39,40} These equations are derived under the assumption that the exchange energy is much larger than the anisotropy energy, which is realized in $\text{MnCl}_3(\text{bpy})$. By using the J value evaluated by fitting of magnetic susceptibility ($J/k_B = 31.2$ K), the resulting zero-field splitting parameters are $D/k_B = -1.5$ K and $E/k_B = -0.17$ K, and the g -values are $g_{a^*} = 2.09$, $g_b = 1.92$, and $g_c = 2.07$. The D/J ratio is evaluated to be -0.047 . From this value, $\text{MnCl}_3(\text{bpy})$ might be in the Haldane phase calculated by Tonegawa *et al.*¹⁴ Unfortunately, however, this compound exhibits a long-range order at 11.5 K due to the interchain interactions.

Most experimental AFMR branches are well reproduced by the aforementioned AFMR branches, but the

branches near and above H_{SF} are largely different. The broken lines near the experimental data around H_{SF} are guides for the eyes. Strikingly, ESR signals at 70 GHz and 90 GHz were not detected, and therefore, the branch *possesses* an energy minimum gap at 22 T, which is close to the transition field observed in the magnetization curve for $H\parallel c$. This energy gap at 22 T may originate from staggered magnetic fields caused by the alternately tilted magnetic moments toward the b -axis due to the alternatively tilting MnCl_3N_2 octahedra in the chains,³³ resulting in the alternative inclination of the g -tensor, or the Dzyaloshinskii-Moriya interaction that is thought to be in this compound. These possibilities could be the reasons for the difference between the spin-flop transition fields between the experiment and the calculation (molecular field approximation).

IV. SUMMARY

Magnetic susceptibility, heat capacity, high-field magnetization, and ESR measurements have been performed on single crystals of $\text{MnCl}_3(\text{bpy})$. In a preliminary report,³² the discrepancy between the spin-flop transition field observed by the high-field magnetization experiment on a single crystal sample of $\text{MnCl}_3(\text{bpy})$ were different from the ones expected from the AFMR mode analysis performed by the fitting the high-frequency resonance field data obtained with a powder sample.³³ As reported herein, when using single crystal samples, the observed resonance modes near the spin-flop field are indeed different from those calculated for the antiferromagnetic resonance modes with orthorhombic anisotropy. Instead, the resonance mode has an energy minimum with a small gap at this transition field, and above the transition field, the observed resonance mode is shifted to a lower field. These findings remain for the future work.

ACKNOWLEDGMENTS

This work was supported, in part, by Grants-in-Aid for Scientific Research (No. 24240590, 25246006, and 25220803) from the MEXT, Japan, and by the National Science Foundation through DMR-1405439 (DRT), DMR-1202033 (MWM), and DMR-1157490 (NHMFL).

¹ H. Bethe, Z. Physik **61**, 206 (1930); Z. Physik **74**, 295 (1932).

² L. Hulthén, Arkiv. Mat. Astron. Fysik **26A**, 11 (1938).

³ R.B. Griffiths, Phys. Rev. **133**, A768 (1964).

⁴ F.D.M. Haldane, Phys. Lett. **79**, 464 (1983); Phys. Rev. Lett. **50**, 1153 (1983).

⁵ J.C. Bonner and M.E. Fisher, Phys. Rev. **135**, A640 (1964).

⁶ J. des Cloizeaux and J.J. Pearson, Phys. Rev. **128**, 2131 (1962).

⁷ K. Takeda, S. Matsukawa, and T. Haseda, J. Phys. Soc. Jpn. **30**, 1330 (1971).

⁸ Y. Endoh, G. Shirane, R.J. Birgeneau, P.M. Richards, and S.L. Holt, Phys. Rev. Lett. **32**, 170 (1974).

⁹ M.P. Nightingale and H.W.J. Blöte, Phys. Rev. B **33**, 659 (1986).

¹⁰ S. Todo and K. Kato, Phys. Rev. Lett. **87**, 047203 (2001).

¹¹ H. Nakano and A. Terai, J. Phys. Soc. Jpn. **78**, 014003 (2009).

¹² M. Oshikawa, J. Phys.: Condens. Matter. **4**, 7469 (1992).

- ¹³ U. Schollwöck and T. Jolicoeur, *Europhys. Lett.* **30**, 493 (1995).
- ¹⁴ T. Tonegawa, K. Okamoto, H. Nakano, T. Sakai, K. Nomura, and M. Kaburagi, *J. Phys. Soc. Jpn.* **80**, 043001 (2011).
- ¹⁵ F. Pollmann, E. Berg, A.M. Turner, and M. Oshikawa, *Phys. Rev. B* **85**, 075125 (2012).
- ¹⁶ J.A. Kjäll, M.P. Zaletel, R.S.K. Mong, J.H. Bardarson, and F. Pollmann, *Phys. Rev. B* **87**, 235106 (2013).
- ¹⁷ S.C. Furuya, M. Oshikawa, and I. Affleck, *Phys. Rev. B* **83**, 2244177 (2011).
- ¹⁸ J.P. Renard, M. Verdager, L.P. Regnault, W.A.C. Erkelens, J. Rossat-Mignod, and W.G. Stirling, *Europhys. Lett.* **3**, 945 (1987).
- ¹⁹ K. Katsumata, H. Hori, T. Takeuchi, M. Date, A. Yamagishi, and J.P. Renard, *Phys. Rev. Lett.* **63**, 86 (1989).
- ²⁰ O. Avenel, J. Xu, J.S. Xia, M-F. Xu, B. Andraka, T. Lang, P.L. Moyland, W. Ni, P.J.C. Signore, C.M. van Woerkwina, E.D. Adams, G.G. Ihas, M.W. Meisel, S.E. Nagler, N.S. Sullivan, and Y. Takano, *J. Low Temp. Phys.* **89**, 547 (1992).
- ²¹ S. Ma, C. Broholm, D.H. Reich, B.J. Sternlieb, and R.W. Erwin, *Phys. Rev. Lett.* **69**, 3571 (1992).
- ²² W. Lu, J. Tuchendler, M. von Ortenberg, and J.P. Renard, *Phys. Rev. Lett.* **67**, 3716 (1991).
- ²³ L.C. Brunel, T.M. Brill, I. Zaliznyak, J.P. Boucher, and J.P. Renard, *Phys. Rev. Lett.* **69**, 1699 (1992).
- ²⁴ M. Hagiwara, K. Katsumata, I. Affleck, B.I. Halperin, and J.P. Renard, *Phys. Rev. Lett.* **65** 3181 (1990).
- ²⁵ S.H. Glarum, S. Geshwind, K.M. Lee, M.L. Kaplan, and J. Michel, *Phys. Rev. Lett.* **67** 1614 (1991).
- ²⁶ M. Hagiwara and K. Katsumata, *J. Mag. Mag. Mater.* **140-144**, 1665 (1995).
- ²⁷ H. Yamazaki and K. Katsumata, *Phys. Rev. B* **54**, R6831 (1996).
- ²⁸ Y. Matsushita and Y. Ueda, *Inorg. Chem.* **42**, 7830 (2003).
- ²⁹ M.B. Stone, G. Ehlers, and G.E. Granroth, *Phys. Rev. B* **88**, 104413 (2013).
- ³⁰ G.E. Granroth, M.W. Meisel, M. Chaparala, Th. Jolicoeur, B.H. Ward and D.R. Talham *Phys. Rev. Lett.* **77**, 1616 (1996).
- ³¹ M. Hagiwara, Y. Idutsu, Z. Honda, and S. Yamamoto, *J. Phys.: Conf. Ser.* **400**, 032014 (2012).
- ³² M. Hagiwara, M. Ikeda, Y. Idutsu, S. Kimura, and Z. Honda, *J. Korean Phys. Soc.* **62**, 2046 (2013).
- ³³ M. Hagiwara, S. Shinozaki, A. Okutani, D. Yoshizawa, T. Kida, T. Takeuchi, O.N. Risset, D.R. Talham, and M.W. Meisel, *Physics Procedia* **XX**, in press (2015).
- ³⁴ S.P. Perlepes, A.G. Blackman, J.C. Huffman, and G. Christou, *Inorg. Chem.* **30**, 1665 (1991).
- ³⁵ G.E. Granroth, Ph. D. thesis, University of Florida (1998). <https://archive.org/details/experimentalstud00gran>.
- ³⁶ B. Ward, Ph. D. thesis, University of Florida (1997). <https://archive.org/details/electronicmagnet00ward>.
- ³⁷ S. Yamamoto, *Phys. Lett. A* **213**, 102 (1996).
- ³⁸ Erik Čížmár, O. N. Risset, T. Wang, M. Botko, A. Ahir, M. J. Andrus, J.-H. Park, K. A. Abboud, D. R. Talham, M. W. Meisel, and S. E. Brown, *Phys. Rev. B* **xxx**, submitted (2015).
- ³⁹ M. Date and M. Motokawa, *J. Phys. Soc. Jpn.* **22**, 165 (1967).
- ⁴⁰ J. Kanamori and H. Minatono, *J. Phys. Soc. Jpn.* **17**, 1759 (1962).